TABLE VI

SHEAR FLOW GEOMETRIES AS LIMITING CASES OF HELICAL FLOW[a]

Flow geometry as described in Fig. 3	κ	$V_Z(\kappa, Z)$	$\bar{V}_Z$
a_1	0.999	2	1
b	$0 < \kappa < 1$	determined by iteration for $P' = 0$	1
c	0	—	1
d	0.999	0	1
e	$0 < \kappa < 1$	0	1
f	$0 < \kappa < 1$	0	$0 < \bar{V}_Z < 1$
g	$0 < \kappa < 1$	finite	1
h	0.999	finite	1
a_2	0.999	0	0
i	$0 < \kappa < 1$	0	0

[a] Listing of the corresponding geometry (described with κ) and kinematics (described with the velocity of the inner cylinder $V_Z(\kappa, Z)$ and the average axial velocity $\bar{V}_Z$). Geometries a_1–h are with open, and geometries a_2 and i with closed stream lines.

Due to the parabolical character of the solution procedure for the equation of energy, the helical flow program can be applied only to flows with non-negative velocity components. Thus, axial drag flow in an annulus with nonzero axial pressure gradient (type g) and drag flow in a narrow slit between two parallel plates with nonzero pressure gradient (type h) can be analyzed only up to moderate positive pressure gradients. A solution procedure that allows for back flow is described in the literature [104], but it does not seem to have been applied to these types of flow.

4. *Calculated Results*

There is a large variety of heat transfer problems solvable with the universal shear flow program. Some examples follow, mainly concerning the thermal boundary conditions (Biot number) and the kinematics for various shear flow geometries. Similar examples of helical flow or annular flow calculations have already been published, however, with idealized thermal boundary conditions [85]. In all the examples of this section, the entrance temperature (at $Z = 0$) is taken to be $\vartheta_e(R) = 0$.

The *thermal boundary conditions* influence the developing temperatures and velocities to a large extent. In analytical studies generally, idealized conditions are assumed, i.e., isothermal or adiabatical wall; in real flow

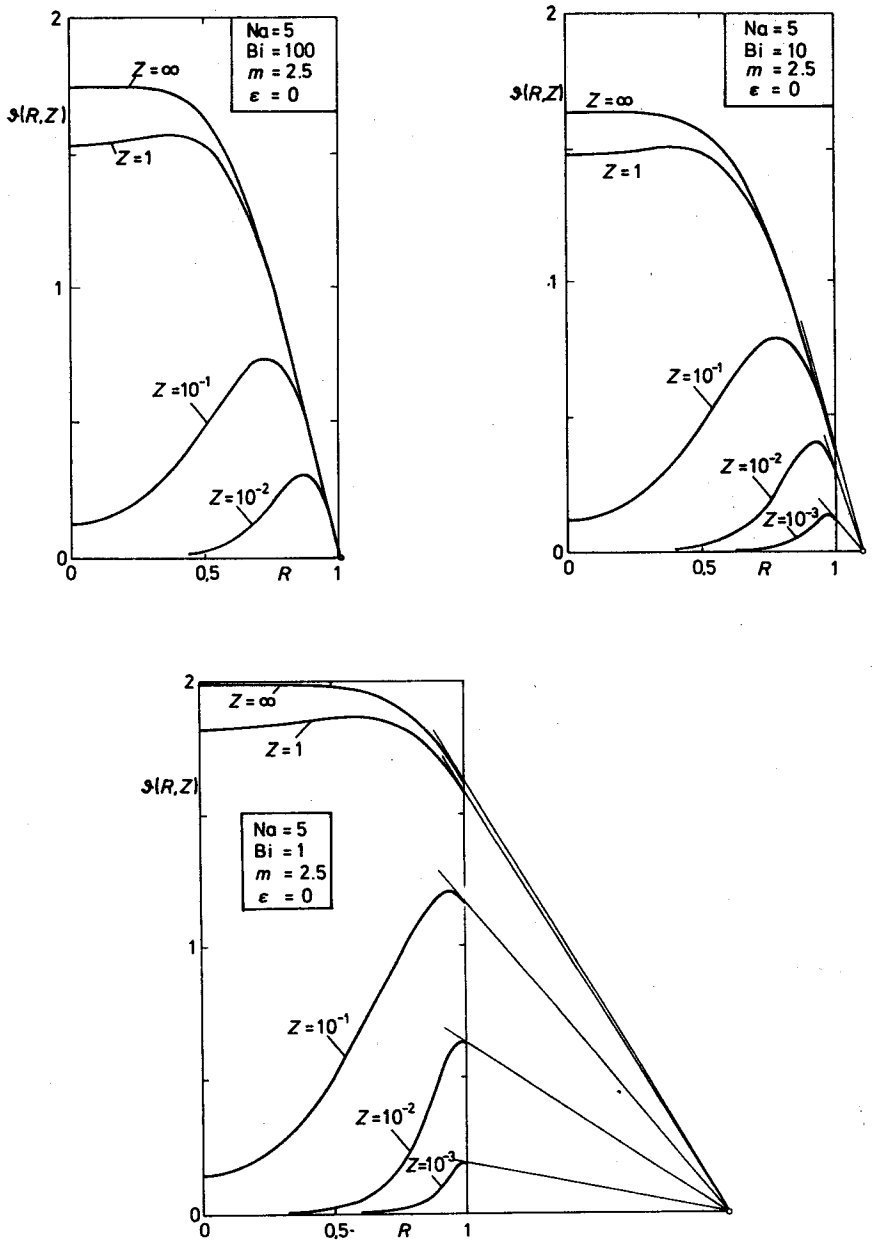

FIG. 8. Influence of the thermal boundary condition, described by a guide point outside the channel given by Bi and $\vartheta_s = 0$, on the developing temperature field in pipe flow. Bi = 100 is close to the isothermal wall condition, while Bi = 1 causes large changes of the wall temperature.

situations the thermal boundary condition is somewhere between the two. The strength of the Biot number in describing a more realistic kind of boundary condition will be demonstrated on pipe flow: the fluid supposedly enters the pipe at a constant temperature equal to the temperature of the surroundings ($\vartheta_e = \vartheta_s = 0$).

Due to viscous dissipation, the temperatures increase in flow direction (Fig. 8). For Bi = 100, the wall temperature stays nearly constant, while for Bi = 10 and Bi = 1, the wall temperatures already increase in early development. The fully developed temperature at Bi = 10 has a value between that at Bi = 100 and Bi = 1. At *large* Bi the temperature in the layer near the wall is kept low; the viscosity and hence the viscous dissipation is large, and a large temperature gradient is needed to conduct away all newly dissipated energy. At *small* Bi the wall temperatures have to rise significantly before the heat flux at the wall can balance dissipation; the temperature gradient can still be relatively small since the viscosity and hence the viscous dissipation become small at high temperatures. At large Bi the temperatures are high because viscous dissipation is most pronounced. At small Bi the temperatures are high because the conduction toward the surroundings requires large wall temperatures. For intermediate Bi, the fully developed temperature has a minimum.

The corresponding pressure gradient $P'(Z)$ decreases due to the decrease of the temperature dependent viscosity (Fig. 9). The decrease of $P'(Z)$ below its value at the entrance $P'(0)$ is most pronounced at small values of the Biot number, where the wall temperatures increase the most.

The temperature gradient at the wall is defined with the Biot number and an outer temperature difference $\vartheta_s - \vartheta_w$ (see Eq. (2.54)), where $\vartheta_w(Z)$ itself depends, besides the other parameters, on Bi. The dimensionless temperature

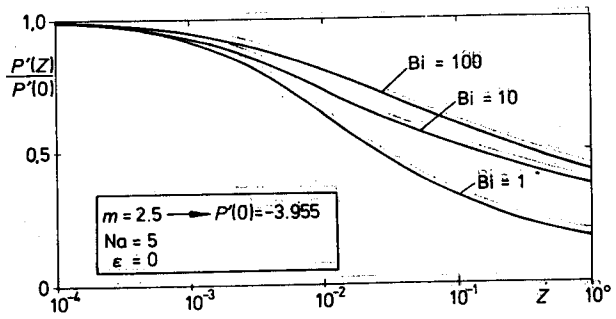

FIG. 9. Pressure gradient in pipe flow at different thermal boundary conditions; decrease due to the thermal development described in the previous figure. The pressure gradient for isothermal pipe flow can be calculated analytically: $P'(0) = -2(m + 3)^{1/m}$.

gradient $[\partial\vartheta(R, Z)/\partial R]_w$ increases with Z till it reaches its fully developed value at about $Z = 1$ (see Fig. 8).

a. Nusselt Number. For engineering calculations, the specific heat flux q often is described by means of the Nusselt number [106]

$$\mathrm{Nu} = \frac{h}{(\Delta T)_{\mathrm{ref}}}\left(\frac{\partial T}{\partial r}\right)_w \tag{2.59}$$

and a characteristic temperature difference $(\Delta T)_{\mathrm{ref}}$. The product $\mathrm{Nu} \cdot k/h$ sometimes is called the heat transfer coefficient. The value of the Nusselt number depends much on the choice of the temperature difference $(\Delta T)_{\mathrm{ref}}$. For flow *without significant viscous* dissipation, one takes it to be the local average temperature difference $(T_w - \bar{T}(Z))$ or the average temperature change $(\bar{T}(Z) - \bar{T}(0))$ in the flow direction. The average temperature of the melt is chosen to be the "cup mixing temperature"

$$\bar{T}(Z) = \frac{2}{1 - \kappa^2}\int_\kappa^1 T(R, Z)V_Z(R, Z)R\,dR \tag{2.60}$$

which would be the temperature of the homogeneous fluid after mixing (constant specific heat per volume assumed).

The Nusselt number in its usual definition is not adequate for describing the wall heat flux in flows with significant viscous dissipation. One disadvantage of the use of Nu is the fact that both $\mathrm{Nu}(Z)$ and $\bar{T}(Z)$ have to be known to calculate the wall heat flux $q(Z)$; the main disadvantage, however, is that in Nu an attempt is made to describe two fairly unrelated quantities as a function of each other, the temperature gradient at the wall and the average temperature difference $(T_w(Z) - \bar{T}(Z))$. This will be explained in the following, using pipe flow as an example.

Figure 10 shows developing temperature profiles in pipe flow, on the left-hand side with negligible viscous dissipation ($\mathrm{Na} = 0.001$) and on the right-hand side with significant viscous dissipation ($\mathrm{Na} = 1$). The wall temperature is *above* the entrance temperature ($\vartheta_e = 0$; $\vartheta_s = 0.1$); developing temperatures at constant wall temperature ($\mathrm{Bi} = \infty$) are drawn as solid lines, while for a thermal boundary condition with $\mathrm{Bi} = 10$ dashed lines are used. For flow *without significant dissipation* ($\mathrm{Na} = 0.001$), the temperature of the fluid gradually approaches the wall temperature; the temperature gradient at the wall (shown in Fig. 11) decreases monotonically till it becomes zero. However, if there is *significant viscous dissipation* ($\mathrm{Na} = 1$), the temperature in the layer next to the wall increases drastically even before the average temperature is changed much. The temperature gradient changes its sign; the fluid heats the wall, even if the average fluid temperature is below the

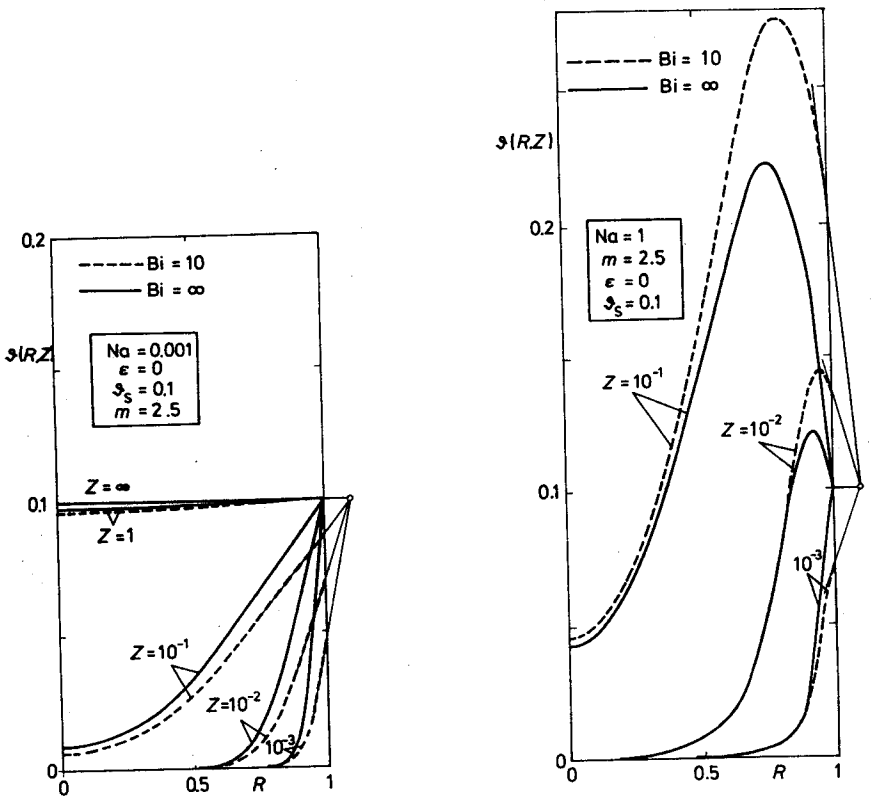

FIG. 10. Calculated temperatures in pipe flow with wall temperatures above the entrance temperature. Comparison of the thermal development without (Na = 0.001) and with (Na = 1) significant viscous dissipation. The wall temperature is taken to be constant (Bi = ∞) or described by a guide point with Bi = 10.

wall temperature. This corresponds to a *negative Nusselt number* or a negative heat transfer coefficient, which is an unrealistic result.

The dimensionless average temperature difference (Fig. 12)

$$\bar{\vartheta}(Z) - \vartheta_w(Z) = \beta(\bar{T}(Z) - T_w(Z)) = \beta\,\Delta\bar{T} \tag{2.61}$$

is negative at the entrance of the pipe (prescribed initial condition) and at least for Bi = ∞, it increases monotonically with Z. For Na = 0.001, the fluid approaches the wall temperature ($\vartheta_\infty = \vartheta_w$); for Na = 1, the average temperature difference goes through zero and approaches a constant value greater than zero. The Nusselt number Nu(Z), which conventionally is defined with this temperature difference, has a singularity when the average

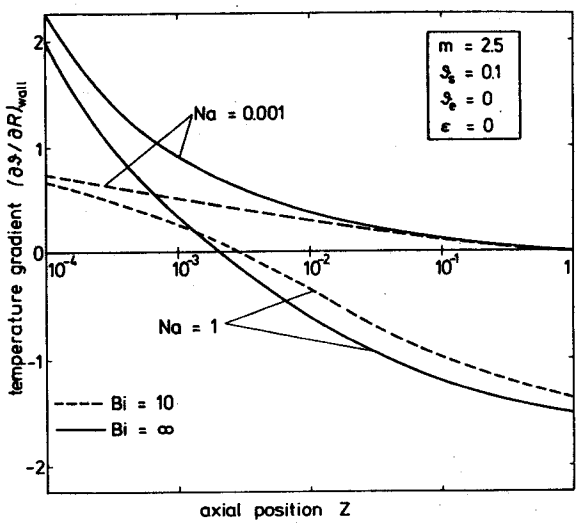

FIG. 11. Wall temperature gradients for pipe flow with viscous dissipation (Na = 1) and without (Na = 0.001). The wall temperature is above the entrance temperature.

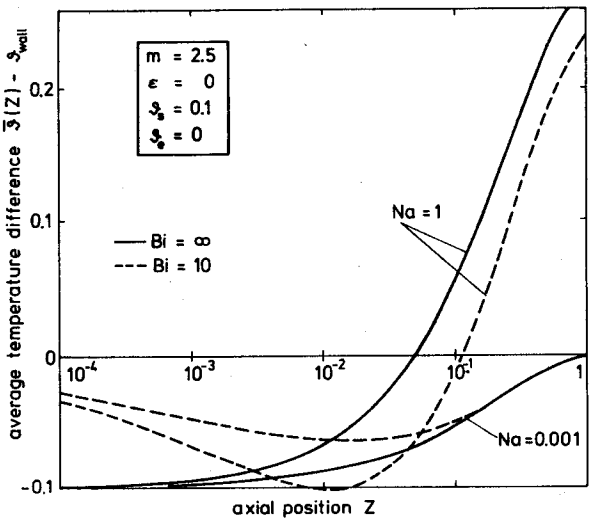

FIG. 12. Development of the difference between the average temperature and the wall temperature in pipe flow with viscous dissipation (Na = 1) and without (Na = 0.001); the wall temperature is above the entrance temperature.

temperature difference $\Delta\bar{T}$ is equal to zero [69, 76, 82]. The specific heat flux at the wall obviously is finite (see the wall temperature gradient in Fig. 11). This seeming singularity (at Z of $\Delta\bar{T} = 0$) suggests that the usual choice of the reference temperature difference $\Delta\bar{T}$ cannot be applied meaningfully to flow problems with viscous dissipation [69]. The same argument is valid if, instead of a constant wall temperature, a guide point is chosen outside the channel, see Figs. 10–12 with Bi = 10.

In the definition of the Nahme number (Eq. (2.55)), β^{-1} is taken to be a characteristic temperature difference, and for defining a Nusselt number for flow with viscous dissipation one similarly may take

$$(\Delta T)_{\text{ref}} = \beta^{-1}. \tag{2.62}$$

Introducing this reference temperature difference into Eq. (2.59), the Nusselt number becomes

$$\text{Nu} = h\beta(\partial T/\partial r)_{\text{w}} = (\partial\vartheta/\partial Y)_{\text{w}}, \tag{2.63}$$

and it then is *identical with the temperature gradient at the wall.* Equation (2.63) seems to be an adequate definition of Nu for flow with viscous dissipation. The relation between Nu and Bi is given together with Eq. (2.54). For fluids with practically temperature-*independent* properties, an adequate definition of the Nusselt number for dissipative flow can be made by means of the "recovery temperature" [98, p. 417].

b. Expansion Cooling. In steady flow of compressible fluids with nonzero pressure gradient, the density will change in the flow direction; the equation of energy, Eq. (1.7), contains a term that describes the cooling or heating due to those density changes

$$\epsilon T \, Dp/Dt,$$

where ϵT can be determined from Eq. (1.10). In the example of Fig. 13 the influence of expansion cooling is shown on developing temperature profiles in pipe flow (with $\vartheta_{\text{e}} = \vartheta_{\text{w}} = 0$). Values of $\epsilon T = 0, 0.1, 0.2, 0.3$ have been used since values of this magnitude can be evaluated from equilibrium thermodynamic data of molten polymers at rest. The applicability of equilibrium data to regions of rapid pressure changes is still an open question.

c. Thermal Development. For constant inlet temperature equal to the temperature of the surroundings, the average temperature increases during the development of the temperature field with increasing Z. The temperature is fully developed at $Z = 0.5$–2. Although the absolute value of the average temperature depends on the power law exponent m, or Na, and on Bi, the relative development is nearly the same for the different examples of pipe

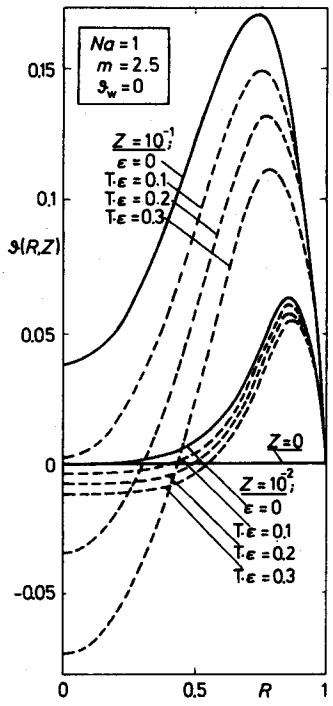

FIG. 13. Calculated temperature profiles in a pipe with constant wall temperature equal to the entrance temperature. The magnitude of ϵT determines the amount of cooling due to expansion with decreasing pressure p; T is the absolute temperature.

flow (Fig. 14). In annular flow, however, the relative thermal development depends on the thermal boundary conditions (Fig. 15); if the dissipated heat can be conducted to both walls ($Bi_i = -10^2$; $Bi_a = 10^5$), the developing length is much smaller than if one wall is nearly adiabatical ($Bi_i = -1$; $Bi_a = 10^5$). For Newtonian fluids ($m = 1$), the channel length required for thermal development is shorter than for fluids with shear dependent viscosity ($m = 3$; $m = 5$, for instance).

d. Zero Pressure Gradient or Zero Wall Shear Stress. The versatility of the program will be demonstrated on some velocity profiles of isothermal flow in an annulus, including the limiting cases of a plane slit ($\kappa \to 1$) and pipe ($\kappa = 0$). Annular flow with zero velocity gradient at the inner wall (which also means zero shear stress at the inner wall) can be achieved with the appropriate pressure gradient and the appropriate velocity $V_Z(\kappa)$ at the inner wall (Fig. 16). An application of this type of velocity field could be die flow in the wire coating process: operating at low shear stress at the surface of the wire prevents ruptures of the wire. If the pressure gradient in the annulus

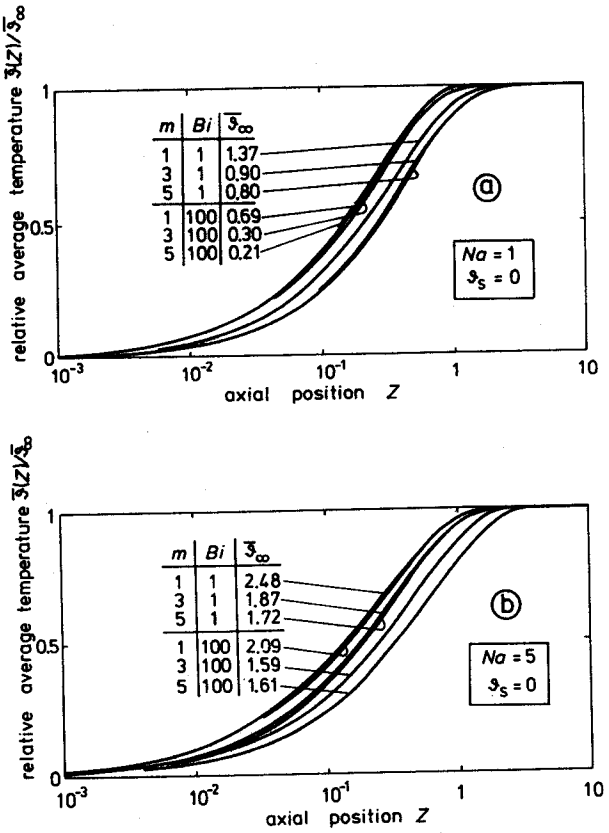

FIG. 14. Development of the average temperature in pipe flow at different Bi and m; (a) at Na = 1 and (b) at Na = 5.

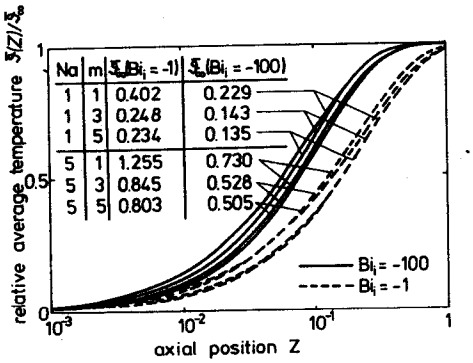

FIG. 15. Development of the average temperature in annular Poiseuille flow at different Bi_i, Na, and m. $\kappa = 0.5$; $\epsilon = 0$.

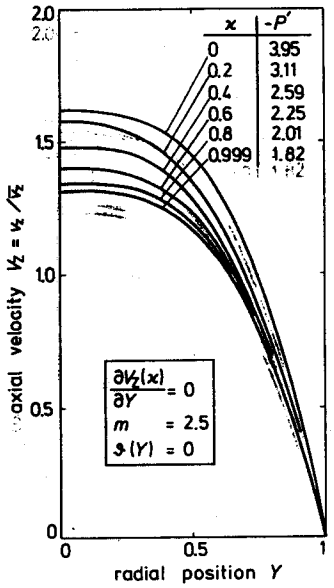

FIG. 16. Calculated velocities and pressure gradients for isothermal axial flow in an annulus with zero shear stress at inner wall. Parameter is the ratio of radii κ.

is prescribed to be zero ($P' = 0$), the axial velocity of the inner cylinder $V_Z(\kappa)$ has to be the larger, the smaller κ is (Fig. 17); for a plane slit ($\kappa \to 1$), the velocity gradient is constant and the velocity of the moving wall is twice the average velocity, obviously. Taking different values $V_Z(\kappa)$ in an annulus of $\kappa = 0.4$ (Fig. 18), the pressure gradient P' adopts positive or negative values. A zero shear stress at the inner wall or a zero pressure gradient at *isothermal* flow does not mean that this condition applies to the whole flow channel: due to the *thermal development* the velocity changes, and accordingly a nonzero shear stress at the inner wall or a nonzero pressure gradient arises.

5. *Experimental Studies*

The main motivations for undertaking experimental studies on heat transfer in steady shear flow with open stream lines seem to be:

investigating the validity of the assumptions made in the analytical studies;
information on the thermal boundary conditions, i.e., values of Bi in different applications.

The flow geometries chosen for experiments were pipe flow and helical flow (see Table V). The measurable quantities were the flow rate, the pressure

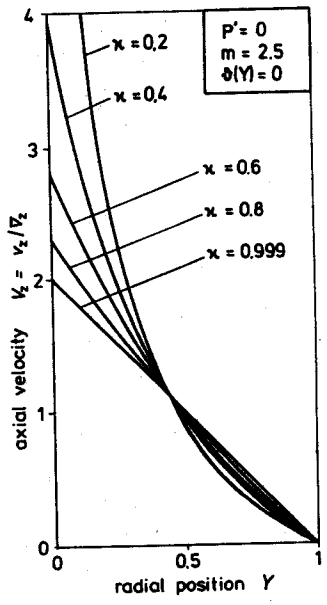

FIG. 17. Calculated isothermal velocity profiles in an annulus at zero pressure gradient. Parameter is the ratio of radii κ.

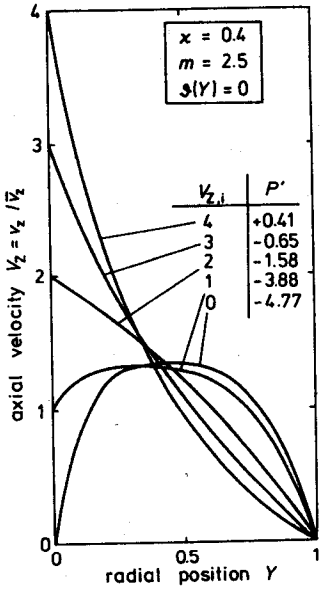

FIG. 18. Calculated isothermal velocity profiles in an annulus of $\kappa = 0.4$. Depending on the values $V_{z,i}$, the pressure gradient P' adopts positive or negative values.

profile, the radial temperature distribution at the inlet and at the exit, the thermal boundary conditions; additionally, for helical flow one could measure the torque and the angular velocity of the cylinders. As input data for the numerical program one needs the flow rate (or a pressure gradient), the properties of the polymer (viscosity $\eta(\dot{\gamma}, T)$, thermal diffusivity $a(T)$, thermal conductivity $k(T)$, density $\rho(p, T)$), the melt temperature at the inlet $T_e(r)$, and two boundary conditions each for the temperature and the velocity fields. The other data can be used for a check on the validity of the numerical solution. Several of the published experimental studies do not specify the data needed for comparing with analytical solutions.

While wall temperatures can be measured quite accurately, the temperature measurements in the flowing molten polymer always contain some systematic errors. A thermocouple mounted on the tip of a probe is placed into the melt stream. The probe is supposed to adopt the melt temperature as closely as possible (zero temperature gradient in the polymer layer next to the probe). Apart from distorting the velocity profile by introducing the probe into the flow, two effects are influencing the temperature measurement: heat conduction along the probe, which requires a heat flux and a temperature gradient in the polymer layer next to the wall of the probe, and viscous dissipation in the polymer around the probe.

The error due to conduction along the probe can be excluded by setting the base temperature, where the probe is mounted to the wall of the channel, equal to the temperature at the tip of the probe [107, 108]. The error due to dissipation cannot be avoided, but it can be kept small by measuring the melt temperature at positions of very low velocities, i.e., after slowing down the flow in a wide channel and then calculating back to the corresponding temperatures at the exit of the narrow channel by means of the stream function [91, 109]. Van Leeuwen [110] studied the applicability of different probe geometries and found that a probe that is directed upstream parallel to the streamlines of the undisturbed flow gives the most accurate temperature data of the melt.

Gerrard *et al.* [67] pumped a Newtonian fluid (oil) through a narrow capillary (r_a = 0.425 mm and 0.208 mm, $33 \leq l/r_a \leq 459$). They measured the pressure drop, the flow rate, the inlet temperature, the wall temperatures, and the radial temperature distribution at the exit. The calculated values of the pressure drop and the temperature at the exit reportedly agree with the measured values within 5%. The viscosity was taken to be a function of temperature; expansion cooling was neglected in the analysis.

Mennig [72] extruded polymer melt (low density polyethylene) through a capillary (r_a = 3.5 mm, l/r_a = 225.7) at adiabatic wall conditions. Measured quantities were the temperature in the center of the entering polymer stream, the wall temperature distribution, the radial temperature distribution at the

exit, and the total pressure drop. The calculated values of the wall temperatures and of the radial temperature distribution exceeded the measured values by about 5%. The viscosity has been taken to be a function of shear rate and of temperature; expansion cooling has been included in the analysis.

For capillary flow, Daryanani *et al.* [75] measured the average heat flux through the wall using an electrical compensation method. From the total pressure drop and the heat flux through the wall, they calculated the average temperature increase between entrance and exit of the capillary.

Winter [91] extruded a polymer melt (low density polyethylene) through an annulus ($\kappa = 0.955$ and 0.972) with rotating inner cylinder. The measured quantities were the mass flow rate, the pressure distribution, the rotational speed of the inner cylinder, the radial temperature distribution at the entrance and at the exit, four temperatures each at the inner and at the outer wall. As shown in Fig. 19 the developing temperatures have been calculated beginning with the measured temperature distribution at the inlet. For the exit temperature distribution, measured and calculated values agreed up to $Y \approx 0.75$ within 5% of the temperature increase (at the outer wall, $0.75 \leq Y \leq 1$ the temperature distribution has not been desribed sufficiently with only four temperature readings). The measured and calculated pressure gradients agree within 8%. Expansion cooling has been neglected in the analysis.

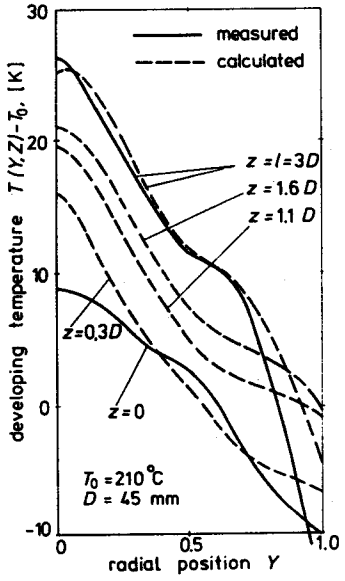

FIG. 19. Comparison of measured and calculated temperature profiles in helical flow [91].

C. SHEAR FLOW WITH CLOSED STREAM LINES

The shear flow geometries with closed stream lines studied most widely are circular Couette flow and its limiting case, i.e., plane Couette flow ($\kappa \to 1$). The fluid is sheared in the annular gap between two concentric cylinders in relative rotation to each other (Fig. 20). The axial velocity component v_z is zero. At time $t = 0$, the Couette system is started from rest at isothermal conditions with a step in shear rate ($\dot{\gamma}(t \leq 0) = 0$ and $\dot{\gamma}(0 < t) = \dot{\gamma}_0 = \text{const}$); alternatively the system might be started with a step in shear stress.

Three types of development are superimposed on each other, each of them on a different time scale:

Kinematic development: The fluid has to be accelerated until it reaches a velocity and a shear rate independent of time. The kinetic development can be calculated for a Newtonian fluid; a practically constant velocity field is reached after [111]

$$t = \rho h^2/16\eta \tag{2.64}$$

(h is the gap width, η the constant Newtonian viscosity, and ρ the density). For viscoelastic liquids an estimate on the duration of kinematic develop-

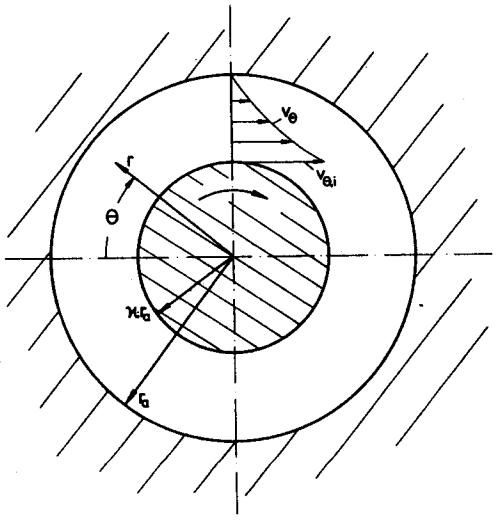

FIG. 20. Flow geometry of circular Couette flow.

ment can be made from the loss and the storage modules G'' and G' measured in periodic shear experiments at frequency $\omega = 1/t$ [112]

$$t \gg h(\rho/G'')^{1/2} \qquad \text{or} \qquad t \gg h(\rho/G')^{1/2} \tag{2.65}$$

For startup experiments on polymer melts, the kinematic development generally is assumed to be completed before the rheological and the thermal development has actually started.

Rheological development: The viscosity $\eta(\dot{\gamma}, T, t)$ needs some time of deformation at constant shear rate, until it adopts a constant value.

Thermal development: Due to viscous dissipation beginning at time $t = 0$, the temperatures in the gap rise until the temperature gradients toward the walls are large enough to conduct away all the newly dissipated energy. Convection does not influence the temperature field because the temperatures along stream lines are constant.

1. *Assumptions and System of Equations*

The assumptions corresponding to the ones listed in Section II.B.1 are:

incompressible fluid with constant thermal conductivity and diffusivity;
no change in z direction;
rotational symmetry ($\partial/\partial\Theta = 0$);
velocity $v_\Theta \neq 0$; $v_r = v_z = 0$;
no slip at walls;
inertia negligible; kinematically developed velocity at $t = 0$;
gravity negligible;
viscosity measured at constant temperatures and constant shear rate gives applicable instantaneous values of the viscosity during temperature changes and during small changes in shear rate; rheologically developed stress at $t = 0$.

The stress equation of motion and the energy equation become

$$0 = \frac{\partial}{\partial r}\left(r^3\eta \frac{\partial}{\partial r}\frac{v_\Theta}{r}\right), \tag{2.66}$$

$$\rho c \frac{\partial T}{\partial t} = \frac{\partial}{r\,\partial r}\left(rk\frac{\partial T}{\partial r}\right) + \eta\left(r\frac{\partial}{\partial r}\frac{v_\Theta}{r}\right)^2. \tag{2.67}$$

The reference values are chosen to be the same as in the helical flow analysis:

$$\bar{v} = v_{\Theta,i}/2; \qquad h = r_a - r_i; \qquad \bar{\dot{\gamma}} = \bar{v}/h; \qquad \bar{\eta} = \eta(\bar{\dot{\gamma}}, T_0).$$

The dimensionless variables are

velocity $V_\Theta = v_\Theta/\bar{v}$,

radial position $R = r/r_a = (1 - \kappa)r/h, \quad \kappa \le R \le 1,$

$$Y = \frac{r - r_i}{r_a - r_i}, \quad 0 \le Y \le 1,$$

shear stress $P_{R\Theta} = \tau_{r\Theta}\frac{h}{\bar{v}\bar{\eta}}$,

temperature $\vartheta = \beta(T - T_0)$.

The dimensionless form of the system of equation reads

$$0 = \frac{\partial}{\partial R}\left(R^3\frac{\eta}{\bar{\eta}}\frac{\partial}{\partial R}\frac{V_\Theta}{R}\right), \tag{2.68}$$

$$\frac{\rho c}{\bar{\rho}\bar{c}}\frac{\partial\vartheta}{\partial \mathrm{Fo}} = (1 - \kappa)^2\left[\frac{\partial}{R\,\partial R}\left(R\frac{k}{\bar{k}}\frac{\partial\vartheta}{\partial R}\right) + \mathrm{Na}\frac{\eta}{\bar{\eta}}\left(R\frac{\partial}{\partial R}\frac{V_\Theta}{R}\right)^2\right]. \tag{2.69}$$

The initial conditions are

$$\vartheta(R, 0) = 0, \qquad V_\Theta(R, 0) = V_{\Theta,0}(R) \tag{2.70}$$

where $V_{\Theta,0}(R)$ is the kinematically developed velocity at the initial temperature. The boundary conditions are

$$\left.\begin{aligned}
\frac{\partial\vartheta(\kappa, \mathrm{Fo})}{\partial R} &= \mathrm{Bi}_i\frac{\vartheta_{s,i} - \vartheta(\kappa, \mathrm{Fo})}{1 - \kappa} + \frac{C_i}{1 - \kappa}\frac{\partial\vartheta(\kappa, \mathrm{Fo})}{\partial \mathrm{Fo}}\\
\frac{\partial\vartheta(1, \mathrm{Fo})}{\partial R} &= \mathrm{Bi}_a\frac{\vartheta_{s,a} - \vartheta(1, \mathrm{Fo})}{1 - \kappa} - \frac{C_a}{1 - \kappa}\frac{\partial\vartheta(1, \mathrm{Fo})}{\partial \mathrm{Fo}}\\
V_\Theta(\kappa, \mathrm{Fo}) &= 2\\
V_\Theta(1, \mathrm{Fo}) &= 0
\end{aligned}\right\} \quad 0 = \mathrm{Fo}. \tag{2.71}$$

The thermal boundary condition is an energy balance of the inner and of the outer wall. The heat flux into the wall is equal to the heat flux out of the wall minus the change of energy stored in the wall. The boundary condition has already been described in Section II.A. It is repeated here to show the complete mathematical problem at once ($\mathrm{Bi}_i < 0$; $\mathrm{Bi}_a, C_i, C_a > 0$).

2. *Dimensionless Parameters*

For a description of most of the dimensionless parameters, the reader is referred to Section II.B.2. The Nahme number, Eq. (2.55), compares the dissipation term and the conduction term of the equation of energy. The

ratio of radii κ shows the influence of curvature, and m describes the shear thinning effect of the viscosity.

Instead of the Graetz number one introduces as a dimensionless variable the Fourier number

$$\mathrm{Fo} = ta/h^2 \tag{2.72}$$

which can be understood as the ratio of the current time of the experiment and the time needed for heat conduction from the center of the channel to the wall. At Fo = 1–4, depending on the thermal boundary conditions, the thermal development is completed. The *Fourier number corresponds to Z* in the heat transfer problem with open stream lines, where one might define an average residence time $\bar{t} = z/\bar{v}_z$:

$$Z = \frac{z}{l}\,\mathrm{Gz}^{-1} = \frac{za}{h^2\bar{v}_z} = \frac{a\bar{t}}{h^2} = \mathrm{Fo}. \tag{2.73}$$

3. *Solution Procedure and Calculated Results*

The Θ component of the equation of motion is the same for annular shear flow with open and with closed stream lines. The *kinematically developed* velocity $V_\Theta(Y, 0)$ at isothermal conditions can be calculated with the existing numerical program of Section II.B without any changes. The same is true for the *thermally developed* case at large times at constant thermal boundary conditions since the conduction and the convection terms are identical in both types of flow. If one replaces Z by Fo and sets $V_Z(Y) = \bar{V}_Z = 10^{-3}$ (which is an arbitrary small value to avoid singularities in the program), even the developing velocity $V_\Theta(Y, \mathrm{Fo})$, temperature $\vartheta(Y, \mathrm{Fo})$, and shear stress $P_{R\Theta}(Y, \mathrm{Fo})$ can formally be taken from the existing program without further considerations; see Table VI. The capacitance parameter, however, has to be included in the thermal boundary condition.

The solution procedure is basically the same for steady shear flow with *open* stream lines and for unsteady shear flow with *closed* stream lines (Couette system), and it would have been possible to treat it in *one* special section in the beginning. For two reasons, however, this has not been done in this study: (1) shear flow with *open* stream lines is much more important for polymer processing; (2) the frequent change from Z to Fo would make the explanations difficult to comprehend. The solution procedure in Section II.B is meant to be an example, and it will not be described repeatedly for the corresponding problem in this section.

The geometry of a cone-and-plate or a plate-and-plate viscometer cannot be described by the existing shear flow program. Turian and Bird [52–54] estimated the temperature effects in cone-and-plate systems by applying the maximal gap width (at the outer radius) to a plane Couette system with

isothermal walls. The radial heat conduction, which might diminish the effect of dissipation, is neglected.

The development of the temperatures in circular Couette flow is a function of the dimensionless parameters Na, Fo, κ, m, and of the thermal boundary conditions. In Figs. 21 and 22, the influence of the geometry on the develop-

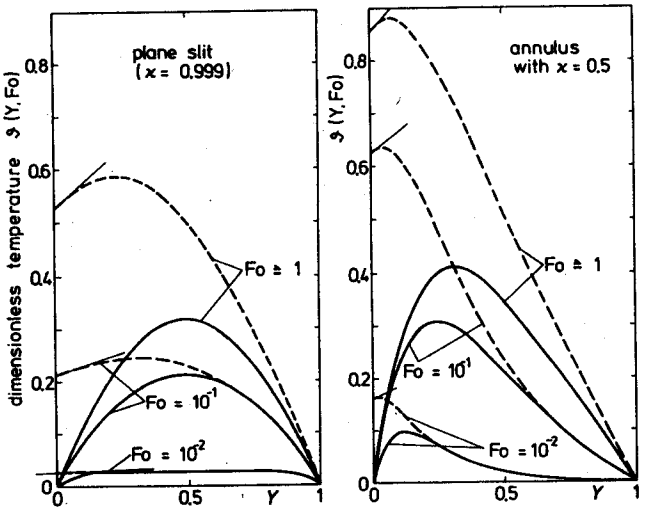

FIG. 21. Comparison of developing temperatures for plane and for circular Couette flow. The outer wall is taken to be isothermal; the inner wall is close to isothermal ($Bi_i = -100$) and close to adiabatical ($Bi_i = -1$). Na = 1; $m = 2$; $C_i = 0$.

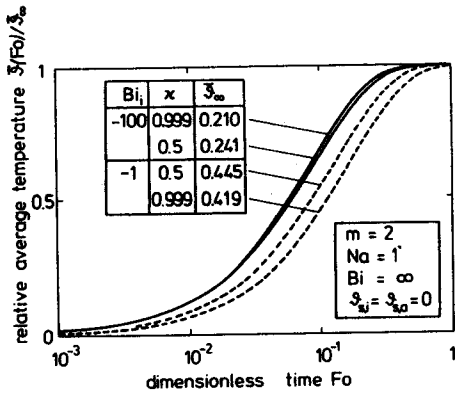

FIG. 22. Development of the average temperature in plane and in circular Couette flow. The solid lines correspond to the development with both walls close to isothermal ($Bi_i = -100$), and for the dashed lines the inner wall has been taken to be close to adiabatical ($Bi_i = -1$). Na = 1; $m = 2$; $C_i = 0$.

ing temperature $\vartheta(Y, \mathrm{Fo})$ will be demonstrated for plane Couette flow ($\kappa \approx 1$) and for circular Couette flow with $\kappa = 0.5$, both with constant temperature of the surroundings equal to the initial temperature ($\vartheta(Y, 0) = \vartheta_{s,i} = \vartheta_{s,a} = 0$); the outer wall is taken to be isothermal ($\mathrm{Bi}_a = \infty$) and the inner wall is taken to be close to isothermal ($\mathrm{Bi}_i = -100$) and close to adiabatic ($\mathrm{Bi}_i = -1$), respectively. The thermal capacitance of the wall is neglected ($C_i = 0$). For the *plane slit* the shear rate and hence the viscous dissipation are nearly uniform. The temperatures rise uniformly until the conduction toward the walls takes more and more heat out of the channel. When the temperature gradients are large enough to conduct away all the newly dissipated energy, the fully developed temperature field is reach. If the inner wall is nearly adiabatical ($\mathrm{Bi}_i = -1$), the temperature gradient has to adopt larger values since nearly all the dissipated energy has to be conducted to the other wall on the outside. The corresponding temperatures for *circular Couette flow* ($\kappa = 0.5$) are asymmetrical through the geometry of the system, additionally to the asymmetry of the thermal boundary condition. The shear rate and the viscous dissipation is much larger at the inner wall than at the outer one. The comparison of the average temperature $\bar{\vartheta}(\mathrm{Fo})$ in Fig. 22 shows that the development is much faster if both walls are cooled instead of one wall being nearly adiabatical ($\mathrm{Bi}_i = -1$).

The thermal development depends on the capacitance of the walls. In an example (Fig. 23) the outer wall of a circular Couette system is taken to be isothermal ($\vartheta(1, \mathrm{Fo}) = 0$); the boundary condition at the inner wall is described by $\mathrm{Bi}_i = -1$, $\vartheta_{s,i} = 0$, and different values of the capacitance parameter C_i. The thermal development is delayed more, the larger the capacitance of the wall is taken to be.

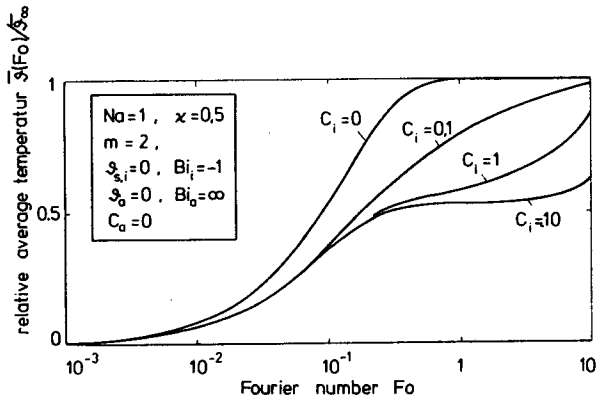

FIG. 23. Thermal development of circular Couette flow depending on the capacitance parameter C_i at the inner wall; the outer wall is taken to be at constant temperature. Na = 1; $m = 2$; $\vartheta_{s,i} = 0$; $\vartheta_{s,a} = 0$; $\mathrm{Bi}_i = -1$.

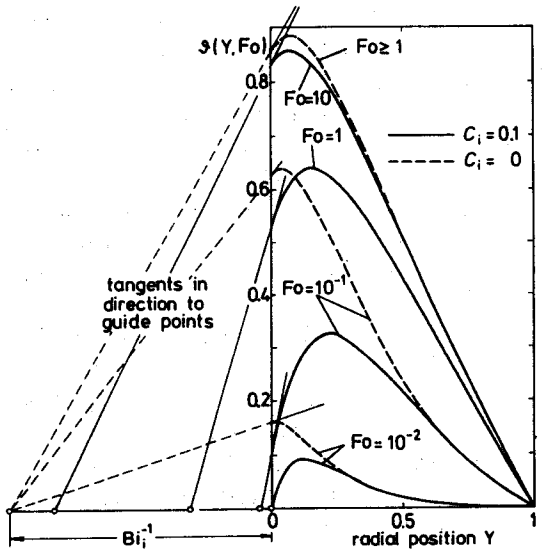

FIG. 24. Developing temperature in circular Couette flow for $C_i = 0$ and $C_i = 0.1$. The temperature of the outer wall is taken to be constant and equal to the initial temperature. $\kappa = 0.5$; Na = 1; $m = 2$; $Bi_i = -1$.

The development of the temperature near the wall is determined by the value of C. For the example in Fig. 24 with $C_i = 0.1$, the guide point initially is very close to the boundary. As the inner wall heats up, the guide point moves away from the boundary until the temperature of both the fluid and the wall reaches its full development. Dissipation and conduction balance and the temperature gradient at the inner wall becomes independent of C_i.

a. Unsteady Plane Shear Flow with Closed Stream Lines. Analytical studies that include the time dependence of the viscosity $\eta(\dot{\gamma}_0, T, t)$ do not seem to be available. Several authors calculated the developing temperature field in plane Couette flow of fluids with a viscosity independent of time:

Gruntfest [89]: $$\eta(T) = \eta(T_0)e^{-\beta(T-T_0)},$$

Krekel [86]: $$\eta(\dot{\gamma}, T) = \frac{A}{\dot{\gamma}} \sinh^{-1}\left(\frac{\dot{\gamma}}{C(T)}\right),$$

Powell and Middleman [92]: $$\eta = \text{const.},$$

Winter [88]: $$\eta(\dot{\gamma}, T) = \frac{\eta(\bar{\dot{\gamma}}, T_0)}{1 + \beta(T - T_0)}\left(\frac{\dot{\gamma}}{\bar{\dot{\gamma}}}\right)^{(1/m)-1}.$$

Practical applications of their studies are the Couette rheometer [88, 89, 92] and a shearing device for breaking up particles suspended in a fluid [86].

For the following example the assumption about the fully developed stress at $t = 0$ will be lifted. A Couette system is kept at rest, and the stress in the system is zero. At time $t = 0$ a shear experiment with constant shear rate is started. The shear stress $\tau_{12}(t)$ is found experimentally (see for instance [113]) to be governed by a time-dependent viscosity that increases gradually, goes through a maximum, and approaches a constant value. If these viscosity data are available, they might be used in the numerical program. For demonstrational purposes, the viscosity curve is approximated by

$$\eta(\dot{\gamma}, T, t) = \underbrace{[\bar{\eta}(\dot{\gamma}/\bar{\dot{\gamma}})^{(1/m)-1} e^{-\beta(T-T_0)}]}_{\text{Eq. (2.47)}}(1 - e^{-c_1 t})(1 + c_2 e^{-c_1 t}), \quad (2.74)$$

which qualitatively fits the measured curve shapes. The maximum viscosity is chosen to be three times the viscosity of steady shear flow; the time of the maximum is chosen to be Fo = 0.1, i.e., at about one-tenth of the thermal development time.

The time-dependent viscosity contains an elastic contribution, which, however, is not specified unless one uses a complete rheological constitutive equation. In the calculation of the dissipated energy, the elastic part of the work of the stress is taken to be negligible compared to the viscous part.

The stress growth curve as chosen in Eq. (2.74) is reproduced by the numerical program with Na = 0.001 (dashed lines in Fig. 25). If viscous dissipation is important (Na = 1, for instance) the stress reaches an earlier maximum at a lower value; the general shape of the curve is not changed through the

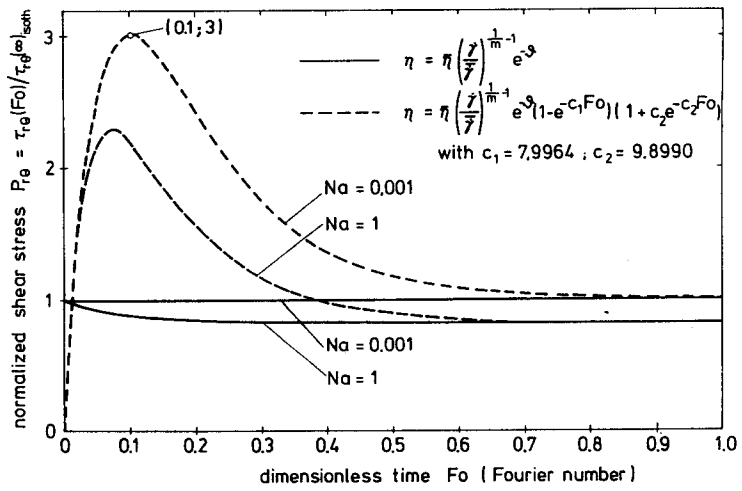

FIG. 25. Thermal influence calculated for the startup experiment of plane Couette flow with time dependent viscosity as described in Eq. (2.74). The walls are taken to be at constant temperature equal to the initial temperature; $m = 2.5$.

effect of dissipation, and rheological and thermal effects seem undistinguishable in stress growth experiments. For comparison, the developing shear stress curves for (rheologically) time-*in*dependent viscosity (as described in Eq. (2.47)) are calculated and drawn as solid lines in Fig. 25.

b. Fully Developed Temperature Field. The fully developed case has drawn much attention (see Table V), which is due to a double-valued solution, found in 1940 by Nahme [44] for plane Couette flow of Newtonian fluids.

The shear stress in fully developed circular Couette flow (including plane Couette flow as a limiting case) cannot exceed a certain value, even if the shear rate is very large; for shear stresses below the maximum possible value, there are always two feasible shear rates $\dot{\gamma}$, a small one at high viscosity and low temperature and a large one at low viscosity and high temperatures. Changes from one shear rate to the corresponding one require large temperature changes, and due to the heat capacity of the system together with the small thermal conductivity of the polymer, oscillations between the two states do not seem possible.

For demonstrating the double-valued solution, Nahme [44] used a dimensionless shear stress τ^* and a dimensionless shear rate $\dot{\gamma}^*$, whose definition can be extended to power law fluids:

$$\tau^* = \mathrm{Na}^{1/(1+m)} P_{R\Theta}(R, \infty)/P_{R\Theta}(R, 0), \tag{2.75}$$

$$\dot{\gamma}^* = \mathrm{Na}^{m/(1+m)}. \tag{2.76}$$

$P_{R\Theta}(R, \infty)$ and $P_{R\Theta}(R, 0)$ are the dimensionless shear stress (see Eq. (2.45)) of the fully developed temperature field and of the isothermal case, respectively; the ratio of the two is independent of R. The dimensionless shear stress

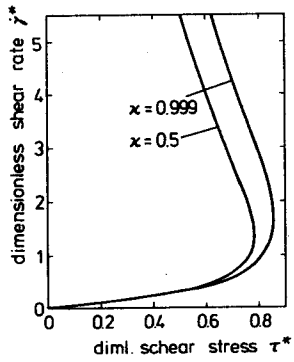

FIG. 26. Shear rate $\dot{\gamma}^*$ as a function of shear stress τ^* (both defined in Eqs. (2.76) and (2.75)) of the fully developed temperature field; the parameter is the geometry.

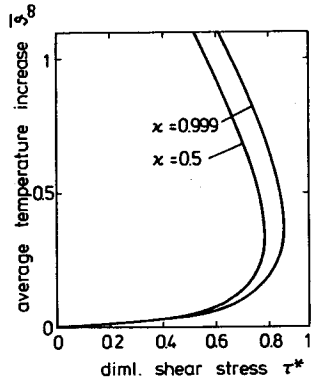

FIG. 27. Average temperature $\bar{\vartheta}_\infty$ of the fully developed temperature field for different geometries of circular Couette flow. Both walls are at constant temperature ($\vartheta_w = 0$); $m = 2$.

$P_{Re}(R, \infty)$ is a monotonically descreasing function of Na, and it cannot be used by itself to demonstrate the double-valued solution. As an example, in Figs. 26 and 27 the double-valued solution $\dot{\gamma}^*(\tau^*)$ and the corresponding average temperature $\bar{\vartheta}_\infty(\tau^*)$ of the fully developed temperature field are shown for circular Couette flow at $\kappa = 0.5$ and $\kappa \approx 1$. Each shear rate $\dot{\gamma}^*$ has only one corresponding temperature $\bar{\vartheta}_\infty$.

4. *Experimental Studies*

The gap width of Couette systems is fairly small; and it is very difficult, if not impossible, to measure the temperature distribution by conventional means. The wall temperatures, however, can be measured quite accurately; other quantities measured are the torque on the system, the rotational speed of the cylinders, and the geometry. The double-valuedness of the shear rate seems to have been verified by Sukanek and Laurence [55] only.

For viscosity measurements, the shear rate is prescribed and the average velocity in plane Couette flow is taken to be $\bar{v} = \dot{\gamma}h/2$. The experiment should be performed at conditions close to isothermal, which means that the Nahme number should be as small as possible:

$$\mathrm{Na} = \frac{\beta \bar{v}^2 \bar{\eta}}{k} = \frac{\beta \bar{\dot{\gamma}}^2 \bar{\eta}}{4k} h^2. \tag{2.77}$$

The Nahme number is proportional to the square of the gap width, i.e., the Couette system should have a very narrow gap. Manrique and Porter [57] built a Couette rheometer with a gap of 5×10^{-3} mm; reportedly they could eliminate the influence of viscous dissipation up to shear rates of $3 \times 10^6\ \mathrm{s}^{-1}$.

III. Elongational Flow; Shear Flow and Elongational Flow Superimposed (Nonviscometric Flow)

The deformation during flow can be understood as a superposition of shear, elongation, and compression. If elongational components and density changes are negligible, the flow is shear flow, and the corresponding heat transfer problems can be analyzed as shown before. However, there are many engineering applications with a flow geometry different from shear flow; how the corresponding heat transfer problems are usually treated will be mentioned briefly. For a more detailed description, the reader will be referred to several examples in the literature.

Other than for shear flow, there is no accepted rheological constitutive equation available for studying heat transfer. The proposed integral and differential constitutive equations are mostly tested in *shear* experiments at *constant temperature*, which might not be significant for *nonviscometric* flow during *temperature changes*. The main reason for not applying constitutive equations of elastic liquids is the fact that they require a detailed knowledge of the kinematics before the stress can be determined. But for other than Couette flow experiments, the kinematics of nonviscometric flows is not known in advance; it has to be calculated simultaneously with the stress. Presently a large emphasis of rheology is on solving nonviscometric flow problems at *constant* temperature. Rheological analysis is not advanced enough to incorporate temperature changes, and the present method of solution for nonviscometric engineering problems is practically identical with the one for steady shear flow, without care of the rheological differences.

Elongational Flow

Up to now, analytical studies on nonisothermal extensional flow have been done by means of a temperature dependent Newtonian viscosity, Eq. (1.13), and constant density. The studies are on melt spinning of fibers (see, for instance, [114, 115]) and on film blowing (see for instance [116, 117]). The measured stress and velocity indicate that the work of the stress $\boldsymbol{\sigma}:\nabla\mathbf{v}$ is very small (at least for film blowing [117]), and the heat transfer seems to be determined by convection with the moving film or thread and by conduction to the cooling medium.

Shear Flow and Elongational Flow Superimposed

In many different channel flows, as they occur in polymer processing, the rate of strain contains elongational components. The fluid elements are

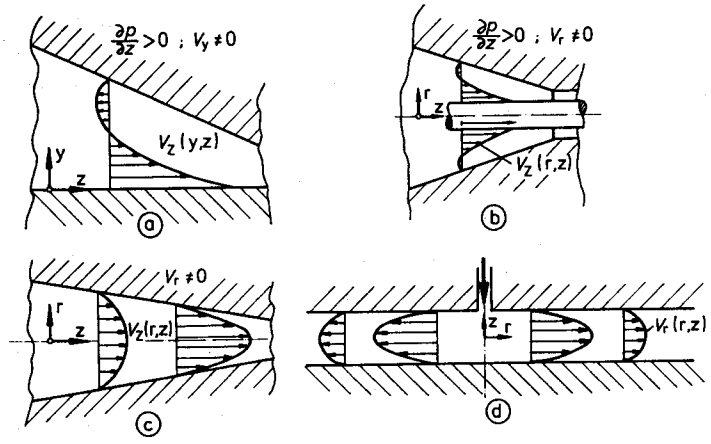

FIG. 28. Examples of converging and diverging flow: (a) Couette flow into a converging slit, which induces a pressure gradient for continuity reasons; (b) Couette flow in a converging annulus; (c) Poiseuille flow into a converging pipe or a converging slit; (d) radial flow in the gap between two parallel plates.

stretched while they are accelerated or slowed down along their paths. Examples (Fig. 28) are Couette flow into a converging slit or annulus, flow in a tapered tube, and radial flow between parallel plates. For describing the stress, one commonly uses the Strokes equation, Eq. (1.13), together with some average viscosity, or one takes the equation of the generalized Newtonian liquid, Eq. (1.14). The results of this kind of calculation seems to give relatively good estimates on temperature changes and viscous dissipation. Examples are heat transfer in screw extruders (see for instance [3, 102, 118–122]), in calendering [123], during mold filling [124–129], and in melt solidification during flow [127–129].

If the deviations from shear flow are small, the stress might still be defined by the viscometric functions. An example of nearly viscometric flow is Poiseuille flow in a pipe with constant but irregular cross section or Poiseuille flow in curved channels with constant cross section; the induced secondary flow in the cross section supports heat transfer toward the walls. The secondary flow, however, is very small. Whereas the improvement on the heat transfer for polymer *solutions* might be up to 30% [130], for *molten* polymers (low density polyethylene in curved pipe) the influence of the secondary flow on the heat transfer was too small to be detectable with temperature probes in the melt [131].

Another example of nearly shear flow occurs in channels near a wall, even if the bulk of the fluid is mainly subjected to deformations other than shear

[132]. For steady flow, the stress at the wall is described by the three viscometric functions and the wall shear rate, which of course can be determined only from the whole flow analysis including the nonviscometric part.

IV. Summary

Heat transfer in flowing molten polymers is largely influenced by rheology, i.e., by the rheological properties of the polymer and by the flow geometry. The rheology of steady shear flow is well understood, and hence the corresponding heat transfer problems can be treated most completely. However, heat transfer studies in flow geometries other than shear are, due to the present lack of an appropriate constitutive equation, only possible in very simplified form.

The most important shear flow geometries are shown to be limiting cases of helical flow, and the corresponding heat transfer problems can be solved with *one* numerical program. Two groups of heat transfer problems are analyzed in the study: heat transfer in steady shear flow with *open stream lines* (represented by helical flow with $\partial/\partial t = 0$) and the corresponding unsteady heat transfer problem with *closed stream lines* (represented by helical flow with $\partial/\partial z = 0$). The problem is completely determined by *six dimensionsless parameters*—the Nahme number; the Graetz number (or the Fourier number, respectively); the ratio of the radii of the annulus; the relative average axial velocity; the power law exponent of the viscosity; and the ratio of length to gap width—together with the boundary conditions.

The commonly used idealized boundary conditions are replaced by the *Biot number* for describing the heat conduction to the surroundings and by the *capacity parameter* for describing the thermal capacity of the wall during temperature changes with time. The conventional definition of the *Nusselt number* is not applicable to heat transfer problems with significant viscous dissipation, and a new definition has to be introduced.

The shear dependence of the viscosity is described by a power law and the temperature dependence by an exponential function. The temperature coefficient of the power law region is shown to be directly related to the activation energy of the zero viscosity.

ACKNOWLEDGMENT

The author thanks Prof. G. Schenkel for his critical advice and many helpful suggestions; he has supported not only this work but also several specific studies of the author which were incorporated here. The author thanks Profs. A. S. Lodge, E. R. G. Eckert, and K. Stephan for

many critical comments and the colleagues G. Ehrmann and M. H. Wagner for helpful discussions on details of the study. The Deutsche Forschungsgemeinschaft is also acknowledged for having enabled the author to spend the time from August 1973 to November 1974 in Madison at the Rheology Research Center which was a fruitful preparation for this work.

NOMENCLATURE

a	thermal diffusivity [m^2/s]	s	wall thickness [m]
Bi	Biot number [–], see Eqs. (2.21) and (2.26)	t	time [s]
		T	temperature [K]
c_p, c_v	specific heat capacity at constant pressure or at constant density [J/kg K]	$\bar{T}$	average temperature [K], see Eq. (2.60)
		v_Θ, v_r, v_z	velocity components [m/s]
C	capacitance parameter of wall [–], see Eqs. (2.26) and (2.30)	$v_{\Theta,i}$	angular velocity at inner wall [m/s]
		$\bar{v}_z$	average velocity in z direction [m/s]
e	internal energy [J/kg]		
E	activation energy [J/g-mole]	$\bar{v}$	reference velocity [m/s], see Eq. (2.38)
Fo	Fourier number, at/h^2 [–]		
Gz	Graetz number, $\bar{v}_z h^2/al$ [–]	V_Θ, V_R, V_Z	dimensionless velocity components $v_\Theta/\bar{v}$, $v_r/\bar{v}$, $v_z/\bar{v}$
h	$r_a - r_i$ = gap width [m]; $h = r_a$ for circular across section	Y	coordinate in r direction, see Eq. (2.32)
k	thermal conductivity [J/m s K]	z, $Z = z/(l\,Gz)$	axial coordinate
		α	pressure coefficient of viscosity [m^2/N], $\eta^{-1}(\partial\eta/\partial p)_{T,\dot{\gamma}}$
l, $L = l/h$	length of the slot		
m	power law exponent, see Eq. (2.47)	β	temperature coefficient of viscosity [K^{-1}], $\eta^{-1}(\partial\eta/\partial T)_{p,\dot{\gamma}}$
M	torque [mN]		
Na	Nahme number, $\bar{v}^2\beta\bar{\eta}/k$ [–], see Eq. (2.55)	$\dot{\gamma}$	rate of strain tensor [s^{-1}]
		$\dot{\gamma}$	shear rate in simple shear flow [s^{-1}]
Nu	Nusselt number [–], see Eq. (2.63)	δ	unit tensor
p	pressure [N/m^2], see Eq. (1.13)	ϵ	coefficient of thermal expansion, $-\rho^{-1}(\partial\rho/\partial T)_p$ [K^{-1}]
P'	dimensionless pressure gradient, see Eq. (2.43)	ϑ	dimensionless temperature, $\beta(T - T_0)$
$P_{R\Theta}$, P_{RZ}	dimensionless shear stress components, see Eq. (2.44) and (2.45)	Θ	azimuth coordinate
		κ	ratio of radii, r_i/r_a
q	specific heat flux at boundary [J/m^2 s]	ρ	density [kg/m^3]
		σ	stress tensor [N/m^2]
r, $R = r/r_a$	radial coordinate (note: in Eqs. (1.9) and (2.12), R is the gas law constant)	τ	extra stress tensor [N/m^2]
		φ	shear angle (see Fig. 1)
		ψ_1, ψ_2	first and second normal stress function in shear flow
r_a, r_i	outer and inner radius of annulus [m]		

INDICES

0	initial state, reference state, or related to the zero-viscosity (in α_0, β_0, E_0)	i, a	inner or outer boundary
		r, R, z, Z, Θ	coordinates
		s	surroundings
∞	fully developed state	w	wall, boundary of channel
e	entrance		

REFERENCES

1. G. Schenkel, "Thermodynamik, Wärmeerzeugung und Wärmeübertragung in der Extrudertechnik," VDI-Bildungswerk BW 2185. Ver. Deut. Ing., Düsseldorf, 1972.
2. G. Schenkel, "Kunststoff Technologie," unpublished lecture notes, Universität Stuttgart (1970).
3. J. R. A. Pearson, *Prog. Heat Mass Transfer* **5**, 73 (1972).
4. G. Schenkel, *Kunstst, Gummi* **7**, 237 and 282 (1968).
5. A. B. Metzner, *Adv. Heat Transfer* **2**, 357 (1965).
6. J. E. Porter, *Trans. Inst. Chem. Eng.* **49**, 1 (1971).
7. P. B. Kwant, Doctoral Thesis, Technische Hogeschool, Delft, 1971.
8. R. B. Bird, W. E. Stewart, and E. N. Lightfoot, "Transport Phenomena," 2nd ed. Wiley, New York, 1962.
9. J. G. Oldroyd, *Proc. R. Soc. London, Ser. A* **200**, 523 (1950).
10. J. G. Oldroyd, *Proc. R. Soc. London, Ser. A* **202**, 345 (1950).
11. H. L. Toor, *Ind. Eng. Chem.* **48**, 922 (1956).
12. R. S. Spencer and R. D. Gilmore, *J. Appl. Phys:* **21**, 523 (1950).
13. S. Matsuoka and B. Maxwell, *J. Polym. Sci.* **32**, 131 (1958).
14. R. S. Spencer and R. F. Boyer, *J. Appl. Phys.* **17**, 398 (1946).
15. R. H. Shoulberg, *J. Appl. Polym. Sci.* **7**, 1597 (1963).
16. D. Hansen and C. C. Ho, *J. Polym. Sci., Part A* **3**, 659 (1965).
17. K. Eiermann, *Kunststoffe* **55**, 335 (1865).
18. P. Lohe, *Kolloid Z. & Z. Polym.* **203**, 115 (1965); **204**, 7 (1965);**205**, 1 (1965).
19. V. S. Bil and N. D. Avtokratowa, *Sov. Plast.* (*Engl. Transl.*) *H***10**, 43 (1966).
20. F. Fischer, *Gummi, Asbest, + Kunstst.* **7**, 728 (1970).
21. W. Knappe, *Adv. Polym. Sci* **7**, 477 (1971).
22. H. Wilski, *Kolloid Z. & Z. Polym.* **248**, 861 (1971).
23. J. C. Ramsey, A. L. Fricke, and J. A. Caskey, *J. Appl. Polym. Sci.* **17**, 1597 (1973).
24. K. Hohenemser and W. Prager, *Z. Angew. Math. Mech.* **12**, 216 (1932).
25. W. O. Criminale, J. L. Ericksen, and G. L. Filbey, *Arch. Ration. Mech. Anal.* **1**, 410 (1958).
26. A. S. Lodge, "Body Tensor Fields in Continuum Mechanics, with Applications to Polymer Rheology," Academic Press, New York, 1974.
27. J. Meissner, *Kunststoffe* **61**, 516 (1971).
28. J. Meissner, *Proc. Int. Congr. Rheol., 4th, 1963* Vol. 3, p. 437 (1965).
29. V. Semjonow, *Adv. Polym. Sci.* **5**, 387 (1968).
30. W. Ostwald, *Kolloid-Z.* **36**, 99 (1925).
31. G. V. Vinogradov and A. Y. Malkin, *J. Polym. Sci., Part A* **2**, 2357 (1964).
32. K. H. Hellwege, W. Knappe, F. Paul, and V. Semjonow, *Rheol. Acta* **6**, 165 (1967).
33. L. Christmann and W. Knappe, *Colloid Polym. Sci.* **252**, 705 (1974).
34. M. D. Hersey, *Physics* (*N.Y.*) **7**, 403 (1936).
35. H. Hausenblas, *Ing.-Arch.* **18**, 151 (1950).
36. E. A. Kearsley, *Trans. Soc. Rheol.* **6**, 253 (1962).
37. D. D. Joseph, *Phys. Fluids* **7**, 1761 (1964).
38. B. Martin, *Int. J. Non-linear Mech.* **2**, 285 (1967).

39. J. C. J. Nihoul, *Ann. Soc. Sci. Bruxelles, Ser. I* **85**, 18 (1971).
40. P. C. Sukanek, *Chem. Eng. Sci.* **26**, 1775 (1971).
41. P. C. Sukanek and R. L. Laurence, *Ann. Soc. Sci. Bruxelles, Ser. T* **86**, II, 201 (1972).
42. H. Schlichting, *Z. Angew. Math. Mech.* **31**, 78 (1951).
43. R. E. Colwell, in "Computer Programs for Plastics Engineers" (I. Klein and D. I. Marshall, eds.), p. 183. van Nostrand-Reinhold, Princeton, New Jersey, 1968.
44. R. Nahme, *Ing.-Arch.* **11**, 191 (1940).
45. J. Gavis and R. L. Laurence, *Ind. Eng. Chem., Fundam.* **7**, 232 and 525 (1968).
46. R. M. Turian, *Chem. Eng. Sci.* **24**, 1581 (1969).
47. J. C. J. Nihoul, *Phys. Fluids* **13**, 203 (1970).
48. P. C. Sukanek, C. A. Goldstein, and R. L. Laurence, *J. Fluid Mech.* **57**, 651 (1973).
49. R. Kumar, *J. Franklin Inst.* **281**, 136 (1966).
50. J. M. Wartique and J. C. J. Nihoul, *Ann. Soc. Sci. Bruxelles, Ser. T*, **83**, III, 361 (1969).
51. G. Palma, G. Pezzin, and L. Busulini, *Rheol. Acta* **6**, 259 (1967).
52. R. B. Bird and R. M. Turian, *Chem. Eng. Sci.* **17**, 331 (1955).
53. R. M. Turian and R. B. Bird, *Chem. Eng. Sci.* **18**, 689 (1963).
54. R. M. Turian, *Chem. Eng. Sci.* **20**, 771 (1965).
55. P. C. Sukanek and R. L. Laurence, *AIChE J.* **20**, 474 (1974).
56. D. D. Joseph, *Phys. Fluids* **8**, 2195 (1965).
57. L. Manrique and R. S. Porter, *Polym. Prepr. Am. Chem. Soc., Div. Polym. Chem.* **13** 992 (1972).
58. H. Zeibig, *Rheol. Acta* **1**, 296 (1958).
59. G. M. Bartnew and W. W. Kusnetschikowa, *Plaste Kautsch.* **17**, 187 (1970).
60. B. Martin, "Heat Transfer Coupling Effects Between a Dissipative Fluid Flow and its Containing Metal Boundary Conditions," Reprint of the European Working Party on non-Newtonian Liquid Processing (1970).
61. H. D. Kurz, "Programm für die Berechnung der Druck- und Schleppströmung im ebenen Spalt." Studienarbeit Inst. für Kunststofftechnik, Universität Stuttgart, 1973.
62. H. C. Brinkman, *Appl. Sci. Res., Sect. A* **2**, 120 (1951).
63. R. B. Bird, *SPE J.* **11**, No 7, 35 (1955).
64. H. L. Toor, *Trans. Soc. Rheol.* **1**, 177 (1957).
65. R. E. Gee and J. B. Lyon, *Ind. Eng. Chem.* **49**, 956 (1957).
66. J. Schenk and J. van Laar, *Appl. Sci. Res. Sect. A* **7**, 449 (1958).
67. J. E. Gerrard, F. E. Steidler, and J. K. Appeldorn, *Ind. Eng. Chem., Fundam.* **4**, 332 (1965); **5**, 260 (1966).
68. J. E. Gerrard and W. Philippoff, *Proc. Int. Congr. Rheol., 4th, 1963* Vol. 2, p. 77 (1965).
69. K. Stephan, *Chem.-Ing.-Tech.* **39**, 243 (1967).
70. R. A. Morette and C. G. Gogos, *Polym. Eng. Sci.* **8**, 272 (1968).
71. H. Schlüter, Doctoral Thesis, Technische Universität, Berlin, 1969.
72. G. Mennig, Doctoral Thesis, Universität Stuttgart, 1969; *Kunststofftechnik* **9**, 49, 86, and 154 (1970).
73. N. Galili and R. Takserman-Krozer, *Isr. J. Technol.* **9**, 439 (1971).
74. G. B. Froishteter and E. L. Smorodinsky, *Proc. Int. Semin. Heat Mass Transfer Rheol. Complex Fluids*, Int. Center Heat Mass Transfer, Herzeg Novi (1970).
75. R. H. Daryanani, H. Janeschitz-Kriegl, R. van Donselaar, and J. van Dam, *Rheol. Acta* **12**, 19 (1973).
76. G. Forrest and W. L. Wilkinson, *Trans. Inst. Chem. Eng.* **51**, 331 (1973); **52**, 10 (1974).
77. H. H. Winter, *Polym. Eng. Sci.* **15**, 84 (1975).
78. N. Galili, R. Takserman-Krozer, and Z. Rigbi, *Rheol. Acta* **14**, 550 and 816 (1975).
79. G. Mennig, *Kunststoffe* **65**, 693 (1975).
80. E. M. Sparrow, J. L. Novotny, and S. H. Lin, *AIChE J.* **9**, 797 (1963).
81. A. Seifert, Doctoral Thesis, Technische Universität, Berlin, 1969.
82. J. Vlachopulos and C. K. J. Keung, *AIChE J.* **18**, 1272 (1972).

83. A. Brinkmann, Doctoral Thesis, Technische Hochschule, Braunschweig, 1966.
84. H. Rehwinkel, "Strömungswiderstand und Wärmeübergang bei nicht-Newtonschen Flüssigkeiten in Ringkanälen mit rotierendem Innenzylinder," DFG-Abschlussbericht No. 260/24, Deutsche Forschungsgemeinschaft, Bad Godesberg, 1970.
85. H. H. Winter, *Rheol. Acta* **12**, 1 (1973); **14**, 764 (1975).
86. J. Krekel, Doctoral Thesis, Technische Hochschule, Karlsruhe, 1964.
87. H. H. Winter, *Int. J. Heat Mass Transfer* **14**, 1203 (1971).
88. H. H. Winter, *Rheol. Acta* **11**, 216 (1972).
89. I. J. Gruntfest, *Trans. Soc. Rheol.* **7**, 195 (1963).
90. H. W. Cox and C. W. Macosco, *AIChE J.* **20**, 785 (1974).
91. H. H. Winter, Doctoral Thesis, Universität Stuttgart, 1973.
92. R. L. Powell and S. Middleman, *Int. J. Eng. Sci.* **6**, 49 (1968).
93. R. G. Griskey and I. A. Wiehe, *AIChE J.* **12**, 308 (1966).
94. T. H. Forsyth and N. F. Murphy, *Polym. Eng. Sci.* **9**, 22 (1969).
95. R. G. Griskey, M. H. Choi, and N. Siskovic, *Polym. Eng. Sci.* 287 (1973).
96. J. L. Ericksen, *Q. J. Appl. Math.* **14**, 318 (1956).
97. "VDI-Wärmeatlas," 2nd ed., Ver. Deut. Ing., Düsseldorf, 1974.
98. E. R. G. Eckert and R. M. Drake, "Analysis of Heat and Mass Transfer." McGraw-Hill, New York, 1972.
99. J. L. den Otter, *Rheol. Acta* **14**, 329 (1975).
100. E. Uhland, *Rheol. Acta* **15**, 30 (1976).
101. L. Schiller, *Z. Angew. Math. Mech.* **2**, 96 (1922).
102. R. M. Griffith, *Ind. Eng. Chem., Fundam.* **1**, 180 (1962).
103. L. Graetz, *Ann. Phys. Chem.* **18**, 79 (1889).
104. A. D. Gosman, W. M. Pun, A. K. Runchal, D. B. Spalding, and M. Wolfshtein, "Heat and Mass Transfer in Recirculating Flows," Academic Press, New York, 1969.
105. A. G. Fredrickson and R. B. Bird, *Ind. Eng. Chem.* **50**, 347 (1958).
106. W. Nusselt, *Z. Ver. Dsch. Ing.* **54**, 1154 (1910).
107. W. Tychesen and W. Georgi, *SPE J.* **18**, 1509 (1962).
108. H. Janeschitz-Kriegl, J. Schijf, and J. A. M. Telgenkamp, *J. Sci. Instrum.* **40**, 415 (1963).
109. G. Schenkel, DOS 1, 554, 931 (1966).
110. J. van Leeuwen, *Polym. Eng. Sci.* **7**, 98 (1967).
111. H. Schlichting, "Boundary Layer Theory," p. 65. McGraw-Hill, New York, 1955.
112. J. D. Ferry, "Viscoelastic Properties of Polymers," 2nd ed., p. 121. Wiley, New York, 1969.
113. J. Meissner, *Rheol. Acta* **14**, 201 (1975).
114. Y. T. Shah and J. R. A. Pearson, *Ind. Eng. Chem., Fundam.* **11**, 145 (1972).
115. S. Kase, *J. Appl. Polym. Sci.* **18**, 3267 (1974).
116. C. J. S. Petrie, *AIChE J.* **21**, 275 (1975).
117. M. H. Wagner, *Rheol. Acta* **15**, 40 (1976).
118. B. Martin, J. R. A. Pearson, and B. Yates, *Univ. Cambridge, Polym. Process. Res. Cent. Rep.* No. 5 (1969).
119. R. T. Fenner, "Extruder Screw Design," Iliffe, London, 1970.
120. Z. Tadmor and I. Klein, "Engineering Principles of Plasticating Extrusion," Van Nostrand-Reinhold, Princeton, New Jersey, 1970.
121. G. Schenkel, *Kunststofftechnik* **12**, 171 and 203 (1973).
122. R. V. Torner, "Grundprozesse der Verarbeitung von Polymeren," VEB Dtsch. Verlag Grundstoffind. Leipzig, 1974.
123. V. J. Petrusanskij and A. I. Sachaev, Uch. Zap. Yarosl. Tekhnol. Inst. **23** (1971); cited by Torner [122].

124. J. L. Berger and C. G. Gogos, *Polym. Eng. Sci.* **13**, 102 (1973).
125. M. R. Kamal and S. Kenig, *Antec* **18**, 619 (1972).
126. H. H. Winter, *Polym. Eng. Sci.* **15**, 460 (1975).
127. E. Broyer, C. Gutfinger, and Z. Tadmor, *Trans. Soc. Rheol.* **19**, 423 (1975).
128. J. Rothe, Doctoral Thesis, Universität Stuttgart, 1972
129. C. Gutfinger, E. Broyer, and Z. Tadmor, *Polym. Eng. Sci.* **15**, 515 (1975).
130. D. R. Oliver, *Trans. Inst. Chem. Eng.* **47T**, 8 (1969).
131. H. H. Winter, unpublished experiments.
132. B. Caswell, *Arch. Ration. Mech. Anal.* **26**, 385 (1967).
133. H. Rehwinkel, Doctoral Thesis, Technische Universität Berlin (1970).

s to Volume 13

MARTIN
SPALDING
WHITAKER
I. WINTER

Advances in

HEAT TRANSFER

Edited by

James P. Hartnett

Energy Resources Center
University of Illinois
at Chicago Circle
Chicago, Illinois

Thomas F. Irvine, Jr.

Department of Mechanics
State University of New York
at Stony Brook
Stony Brook, New York

Volume 13

1977

ACADEMIC PRESS · New York · San Francisco · London
A Subsidiary of Harcourt Brace Jovanovich, Publishers